

Pyrochlore antiferromagnet with antisymmetric exchange interactions: critical behavior and order from disorder

Gia-Wei Chern

Department of Physics, University of Wisconsin, Madison, Wisconsin 53706, USA

(Dated: October 29, 2018)

We investigate the nature of phase transitions induced by Dzyaloshinskii-Moriya (DM) interactions on a classical pyrochlore antiferromagnet. For both symmetry-allowed antisymmetric exchange interactions, the macroscopic degeneracy due to geometrical frustration is relieved and a long-range magnetic order appears in the ground state. We find an Ising-like phase transition in the case of direct DM interaction which selects a doubly degenerate all-in all-out magnetic order. In the presence of indirect DM coupling, the magnet undergoes an XY-like phase transition into a state with broken Z_6 symmetry. We show that the critical behavior in both cases is modified due to the constrained spin fluctuations in the correlated Coulomb phase. We also demonstrate an interesting order from disorder phenomenon where the system switches between two distinct types of broken Z_6 symmetry.

I. INTRODUCTION

Geometrical frustration refers to the inability of spins to satisfy conflicting interactions simultaneously due to the lattice connectivity.¹ Magnets with strong geometrical frustration exhibit a variety of unusual ground states, elementary excitations, and phase transitions. One of the most intensively studied frustrated systems is the Heisenberg antiferromagnet on the *pyrochlore* lattice. Monte Carlo simulations with interactions restricted to nearest-neighbor spins showed that the magnet remains disordered even at temperatures well below the energy scale of exchange constant.² Contrary to the uncorrelated paramagnetic state, motions of spins in this so called Coulomb phase are subject to a set of local constraints. In the continuum approximation, these local constraints translate to the Gauss's law for a fictitious magnetic field.³⁻⁵

Many interesting properties of the Coulomb phase can be traced to the macroscopic degeneracy in the classical ground state of the pyrochlore magnet. Indeed, minimization of the nearest-neighbor exchange interaction requires that the total spin on every tetrahedron be zero, which still leaves an extensive number of unconstrained degrees of freedom.² This degeneracy in turn makes the magnet susceptible to small perturbations such as anisotropies, dipolar interaction, etc. In general, the frustration is relieved and some sort of long-range order is selected by the dominant perturbations.

Phase transitions taking place in the highly constrained Coulomb phase also exhibit interesting, and sometimes peculiar, behavior. A recurring theme in experiments and numerical simulations has been the appearance of first-order phase transitions, despite that a Landau-type analysis of the symmetry-breaking phase would otherwise predict a continuous one. Discontinuous phase transitions have been observed in pyrochlore antiferromagnet perturbed by magnetoelastic coupling,^{6,7} long-range dipolar interaction,^{8,9} exchange anisotropy,^{10,11} and further-neighbor exchange interactions.^{12,13} It is known that strong fluctuations of

the order parameter could induce a first-order transition, a scenario frequently occurs when the number of components of the order parameter is greater than four.^{14,15} This is indeed the case for most of the phase transitions mentioned above.

The dipolar spin correlations stemming from the strong local constraints also affect the nature of phase transitions from the Coulomb phase.³⁻⁵ As is well known, the long-range dipolar interaction can change the universality class of a magnetic phase transition, modifying its critical behavior to that of a model with short-range interactions in higher spatial dimensions.^{16,17} In a recent study on the effects of the exchange anisotropy, it was demonstrated that Néel ordering from the Coulomb phase indeed displays a critical behavior similar to that of a uniaxial dipolar antiferromagnet.¹⁰

As most broken symmetries observed in pyrochlore lattice are rather complex, it is desirable to study phase transitions which can be described by simple order parameters. In this paper, we investigate critical behavior of magnetic ordering due to asymmetric exchange coupling, or the Dzyaloshinskii-Moriya (DM) interaction.^{20,21} The relevant order parameters have either a Z_2 or Z_6 symmetry, depending on the sign of the DM interaction. Specifically, we study the classical spin Hamiltonian:

$$\mathcal{H} = J \sum_{\langle ij \rangle} \mathbf{S}_i \cdot \mathbf{S}_j + \sum_{\langle ij \rangle} \mathbf{D}_{ij} \cdot (\mathbf{S}_i \times \mathbf{S}_j), \quad (1)$$

where the two terms represent the isotropic exchange and the DM interactions, respectively, between nearest-neighbor spins. In addition to being an interesting spin model in itself, recent studies have revealed the important role of DM interaction in the formation of magnetic spirals^{22,23} and the magnon Hall effect²⁴ observed in the pyrochlore magnets.

By applying the so called Moriya rules,²¹ the possible forms of the coupling vectors \mathbf{D}_{ij} were determined by Elhadj *et al.* up to a multiplicative constant.²⁵ Depending on the sign of this constant, the corresponding DM terms are called direct and indirect DM interactions. The

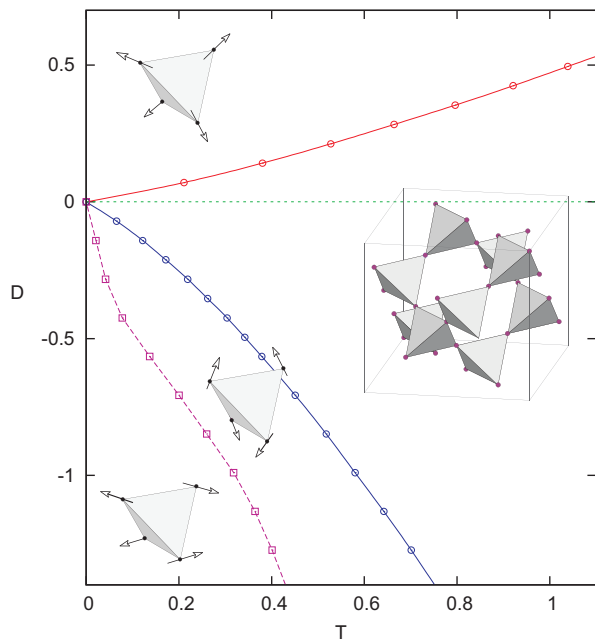


FIG. 1: Phase diagram of Heisenberg antiferromagnet with Dzyaloshinskii-Moriya interaction on pyrochlore lattice (shown in the inset). The ground state of direct DM interaction ($D > 0$) consists of all-in all-out tetrahedra. The ordered phase of indirect DM interaction ($D < 0$) contains two distinct ordered states with broken Z_6 symmetry: noncoplanar and orthogonal structures at high and low T , respectively. The solid and dashed lines denote second-order transition and crossover lines, respectively.

ground states for both forms of the DM interaction were also obtained in Ref. 25. In particular, it was pointed out that indirect DM interaction leaves a continuously degenerate ground state at the mean-field level. Monte Carlo simulations, however, showed that a six-fold degenerate ground state with coplanar spins was selected by thermal fluctuations.^{25,26} Although their preliminary simulations indicated a continuous magnetic ordering for both types of DM interaction, the authors did not touch upon the nature of the phase transitions.

In this paper we performed detailed finite-size scaling to study the critical behavior of model (1). The phase diagram obtained from our extensive Monte Carlo simulations is shown in Fig. 1. Consistent with previous results,²⁵ we found that the direct DM term is minimized by an all-in all-out spin structure, whereas the indirect DM interaction selects orthogonal magnetic orders as $T \rightarrow 0$. By carefully characterizing the symmetry-breaking phase in the indirect DM model, we find a *new* intermediate regime characterized by a magnetic order with noncoplanar spins. A crossover line separates the two different types of broken Z_6 symmetry.

Due to the Z_2 symmetry of the doubly degenerate all-in all-out spin structure, magnetic ordering induced by direct DM interaction ($D > 0$) is expected to be Ising-like. The critical exponents obtained from finite-size scaling

indicate that the transition is indeed close to 3D Ising universality class. We show that the constrained spin fluctuations in the Coulomb phase result in noticeable deviation especially in exponents β and γ .

The case of indirect DM interaction ($D < 0$) is more complicated. Upon lowering the temperature, the magnet undergoes an XY-like transition into a phase with a broken Z_6 symmetry. We introduce a doublet order parameter $\zeta = (\zeta_x, \zeta_y)$ such that the six coplanar ground states correspond to the six corners $\theta_\zeta = n\pi/3$ of a hexagon in the ζ -domain; here n is an integer. Interestingly, below the critical temperature the magnet enters an ordered state characterized by $\theta_\zeta = (n + 1/2)\pi/3$; the corresponding magnetic order consists of noncoplanar spins. As temperature is further lowered the system gradually evolves toward the coplanar magnetic structure. The crossover between the two ordering patterns does not break further symmetries.

The continuous degeneracy of the noncoplanar ground states observed in Ref. 25 manifests itself as an $O(2)$ symmetry of the doublet order parameter ζ . Consequently, both types of broken Z_6 symmetry are entirely due to the entropic effect, or so called order-from-disorder. By explicitly computing the magnon contribution to the free energy, we demonstrate that the above crossover phenomenon is indeed dictated by thermal fluctuations.

The remainder of the paper is organized as follows. In Sec. II, we introduce three antiferromagnetic order parameters to characterize the spin configurations in the ordered phase. The critical behavior of direct and indirect DM interactions is discussed in Secs. III and IV, respectively. A quantitative analysis of the crossover between the two distinct types of broken Z_6 symmetry is presented in Sec. V. Finally we conclude with a discussion of these results in Sec. VI.

II. GROUND-STATE MAGNETIC ORDERS

From the symmetry viewpoint, the DM interaction is allowed on the pyrochlore lattice since the nearest-neighbor bonds are not centrosymmetric.²¹ In Moriya's original theory, the DM term stems from the relativistic spin-orbit interaction.²¹ Regardless of its microscopic origin, the high symmetry of the pyrochlore lattice places strict constraints on the direction of the coupling vectors.²⁵ For a bond oriented along the $[110]$ direction, the vector \mathbf{D}_{ij} points along $[\bar{1}\bar{1}0]$: $\mathbf{D}_{ij} = (\pm D, \mp D, 0)/\sqrt{2}$. The value of \mathbf{D}_{ij} on any other bond can then be found through symmetry transformations.

The expression of the DM interaction could be further simplified using the antiferromagnetic order parameters $\mathbf{L}_1 = (\mathbf{S}_0 + \mathbf{S}_1 - \mathbf{S}_2 - \mathbf{S}_3)/4S$,²² and so on (see Fig. 2 for labeling of the spins), which measure the staggered magnetizations of a tetrahedron. For completeness we also define the ferromagnetic order parameter: $\mathbf{M} = \sum_{i=0}^3 \mathbf{S}_i/4S$. In terms of these variables, Hamiltonian (1) can be recast into a sum over tetrahedra

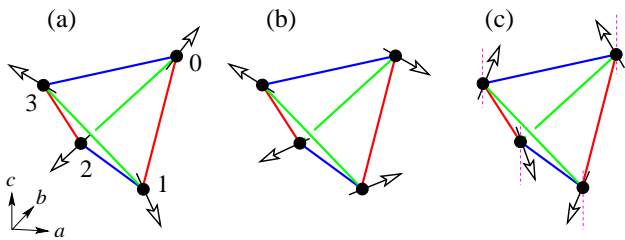


FIG. 2: Magnetic states of a tetrahedron with zero total spin $\mathbf{M} = 0$: (a) all-out, (b) orthogonal, and (c) noncoplanar structures. The three antiferromagnetic vectors \mathbf{L}_1 , \mathbf{L}_2 , and \mathbf{L}_3 measure the staggered magnetizations between the two red, green, and blue bonds, respectively.

$\mathcal{H} = \sum_{\boxtimes} \mathcal{H}_{\boxtimes}$, where the Hamiltonian of a single tetrahedron is

$$\mathcal{H}_{\boxtimes} = 8JS^2 |\mathbf{M}|^2 - 4\sqrt{2}DS^2 (\hat{\mathbf{a}} \cdot \mathbf{L}_2 \times \mathbf{L}_3 + \hat{\mathbf{b}} \cdot \mathbf{L}_3 \times \mathbf{L}_1 + \hat{\mathbf{c}} \cdot \mathbf{L}_1 \times \mathbf{L}_2). \quad (2)$$

Minimization of the exchange energy requires $\mathbf{M} = 0$ on every tetrahedron, which still leaves a macroscopic degeneracy. The remaining degrees of freedom encoded in the three staggered vectors are determined by minimization of the DM term.

Since the vanishing of \mathbf{M} makes the three staggered magnetizations orthogonal to each other and imposes a constraint on their lengths: $\sum_{i=1}^3 |\mathbf{L}_i|^2 = 1$,²² we parameterize the antiferromagnetic order parameters as $\mathbf{L}_i = \phi_i \hat{\mathbf{n}}_i$, where the three $\hat{\mathbf{n}}_i$ form an orthogonal triad and $\phi_i > 0$ denote their lengths. Defining a ‘handedness’ for the triad: $\chi \equiv \hat{\mathbf{n}}_1 \cdot \hat{\mathbf{n}}_2 \times \hat{\mathbf{n}}_3 = \pm 1$, the DM term becomes

$$-\chi DS^2 (\hat{\mathbf{n}}_1 \cdot \hat{\mathbf{a}} \phi_2 \phi_3 + \hat{\mathbf{n}}_2 \cdot \hat{\mathbf{b}} \phi_3 \phi_1 + \hat{\mathbf{n}}_3 \cdot \hat{\mathbf{c}} \phi_1 \phi_2). \quad (3)$$

Note that inversion of the triad $\hat{\mathbf{n}}_i \rightarrow -\hat{\mathbf{n}}_i$ also changes the chirality $\chi \rightarrow -\chi$, reflecting the time-reversal symmetry of the DM interaction. In the following, we focus on the case of a right-handed triad with $\chi = +1$.

For $D > 0$ the DM interaction is minimized first by aligning the triad to the principal crystal axes such that $\hat{\mathbf{n}}_1 = \hat{\mathbf{a}}$, and so on. Minimization of the resultant expression subjecting to the constraint $\sum_{i=1}^3 \phi_i^2 = 1$ yields a ground state with $\phi_1 = \phi_2 = \phi_3 = 1/\sqrt{3}$. The staggered magnetizations are given by

$$\mathbf{L}_1 = (\chi/\sqrt{3}) \hat{\mathbf{a}}, \quad \mathbf{L}_2 = (\chi/\sqrt{3}) \hat{\mathbf{b}}, \quad \mathbf{L}_3 = (\chi/\sqrt{3}) \hat{\mathbf{c}}, \quad (4)$$

with $\chi = \pm 1$ corresponding to the all-out [Fig. 2(a)] and all-in structures, respectively.

The magnet remains frustrated in the presence of the indirect DM interaction, despite a significantly reduced degeneracy. The frustration comes from the fact that absolute minimum of the DM energy with $D < 0$ and $\chi = +1$ requires the unit vectors $\hat{\mathbf{n}}_i$ be antiparallel to the corresponding principal directions, e.g. $\hat{\mathbf{n}}_1 = -\hat{\mathbf{a}}$. However, such a complete anti-alignment is impossible for two

right-handed triads. Numerical minimization yields two inequivalent classes of continuously degenerate ground states. The first set consists of orthogonal spins lying in the plane perpendicular to one of the three cubic axes. The energy of a coplanar state is invariant with respect to uniform rotations of spins about the corresponding cubic axes. For spins perpendicular to the c axis, the magnetic state of the tetrahedron is described by

$$\begin{aligned} \mathbf{L}_1 &= (\cos \phi \hat{\mathbf{a}} + \sin \phi \hat{\mathbf{b}})/\sqrt{2}, \\ \mathbf{L}_2 &= (\sin \phi \hat{\mathbf{a}} - \cos \phi \hat{\mathbf{b}})/\sqrt{2}, \\ \mathbf{L}_3 &= 0. \end{aligned} \quad (5)$$

where the angle ϕ describes the uniform rotation about c axis. As $T \rightarrow 0$, thermal fluctuations select coplanar states with $\phi = 0$ or π .²⁶ The orthogonal structure with spins pointing along the $[110]$ and $[\bar{1}\bar{1}0]$ directions ($\phi = 0$) is shown in Fig. 2(b).

The second set of ground states consists of noncoplanar spins described by order parameters

$$\begin{aligned} \mathbf{L}_1 &= \cos(\theta - \pi/4) \cos \Theta \hat{\mathbf{a}}, \\ \mathbf{L}_2 &= \sin(\theta - \pi/4) \cos \Theta \hat{\mathbf{b}}, \\ \mathbf{L}_3 &= -\sin \Theta \hat{\mathbf{c}}, \end{aligned} \quad (6)$$

where $\Theta = \arctan(\sqrt{2} \sin \theta)$ and θ is a continuous parameter. A tetrahedron with $\theta = 0$ corresponds to orthogonal spins lying in the ab plane. Starting from $\theta = 0$, one can reach the other two inequivalent orthogonal states at $\theta = \pm\pi/4$, where the spins are perpendicular to a and b axes, respectively. As will be discussed in Sec. V, order by disorder at finite temperatures prefers the noncoplanar spins with, e.g. $\theta = \pi/2$, shown in Fig. 2(c).

As first noted in Ref. 27, the coarsed-grained antiferromagnetic order parameters are just the three components of a flux or polarization field introduced in Refs. 4 and 5 to describe the correlated Coulomb phase. This correspondence thus implies that the coarsed-grained staggered fields also obey a dipolar correlation at large distances. A continuum theory of the antisymmetric pyrochlore antiferromagnet is outlined in Appendix A.

Since the DM term does not depend explicitly on \mathbf{M} , a remarkable feature of Hamiltonian (2) is that its ground state is independent of the antiferromagnetic exchange J . However, spin fluctuations in the $J = 0$ and $J \rightarrow \infty$ (Coulomb phase) limits are quite different. In the latter case, minimization of the J term requires spin fluctuations satisfy $\sum_{i \in \boxtimes} \delta \mathbf{S}_i \approx 0$, which in turn result in a dipolar spin correlation at large distances. In the following, we compare the universality class of magnetic ordering in the two limiting cases and show that the critical behavior is indeed modified by the constrained fluctuations in the Coulomb phase.

III. ISING-LIKE PHASE TRANSITIONS: DIRECT DM INTERACTION

The direct DM interaction removes the degeneracy completely and selects a doubly degenerate all-in-all-out ground state. The magnet undergoes a continuous phase transition at a temperature $T_c \sim \mathcal{O}(D)$ as demonstrated by the specific heat curves shown in Fig. 3(a). The peak of the specific heat becomes sharper with increasing system size. However, finite-size scaling of the specific heat is rather difficult due to a nonzero regular component. Instead, by plotting the maximum of heat capacity vs the linear size of the system, we found a power-law dependence $C_{\max} = C_0 + \text{const} \times L^{\alpha/\nu}$, indicating a continuous phase transition. Here we have used an exponent $\alpha/\nu = 0.175$ corresponding to the 3D Ising universality. To further characterize the phase transition, we turn to the finite-size scaling of the order parameter.

In the all-in-all-out structure, spins point along the local $\langle 111 \rangle$ directions with tetrahedra of opposite orientations in the all-in and all-out states, respectively. We introduce an Ising order parameter to characterize this doubly degenerate state:

$$m = \frac{1}{NS} \sum_i \mathbf{S}_i \cdot \hat{\mathbf{e}}_i, \quad (7)$$

where N is the number of spins and $\hat{\mathbf{e}}_i$ points along the local $[111]$ axes, i.e. from the center of type-I tetrahedron to the corresponding corner. The magnetic susceptibility and Binder's cumulant are defined accordingly

$$\chi_m = \frac{N}{T} (\langle m^2 \rangle - \langle |m| \rangle^2), \quad B_{4m} = 1 - \frac{\langle m^4 \rangle}{3\langle m^2 \rangle^2}. \quad (8)$$

The temperature dependence of these variables are shown in Fig. 4 for various linear size L . As can be seen from Fig. 4(a), the order parameter $|m|$ starts to grow below a critical temperature $T_c \approx 0.38J$ estimated from the crossing of the Binder's cumulant shown in Fig. 4(e).

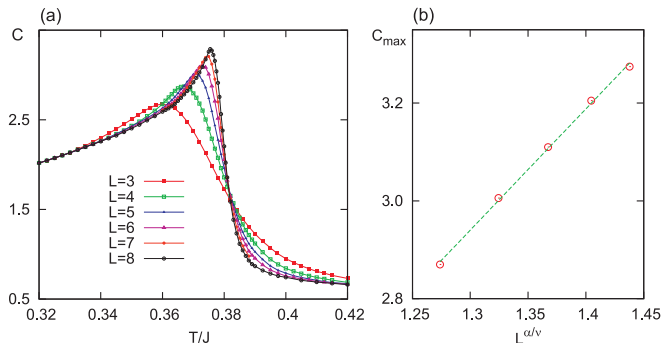


FIG. 3: Monte Carlo simulations for coupling constants $D = 0.14J$. (a) Specific heat $C = (\langle E^2 \rangle - \langle E \rangle^2) / NT^2$ as a function of temperature T for various system sizes. (b) The maximum of the specific heat C_{\max} as a function of $L^{\alpha/\nu}$, where $\alpha/\nu = 0.175$. The number of spins $N = 16L^3$ for a system with linear size L .

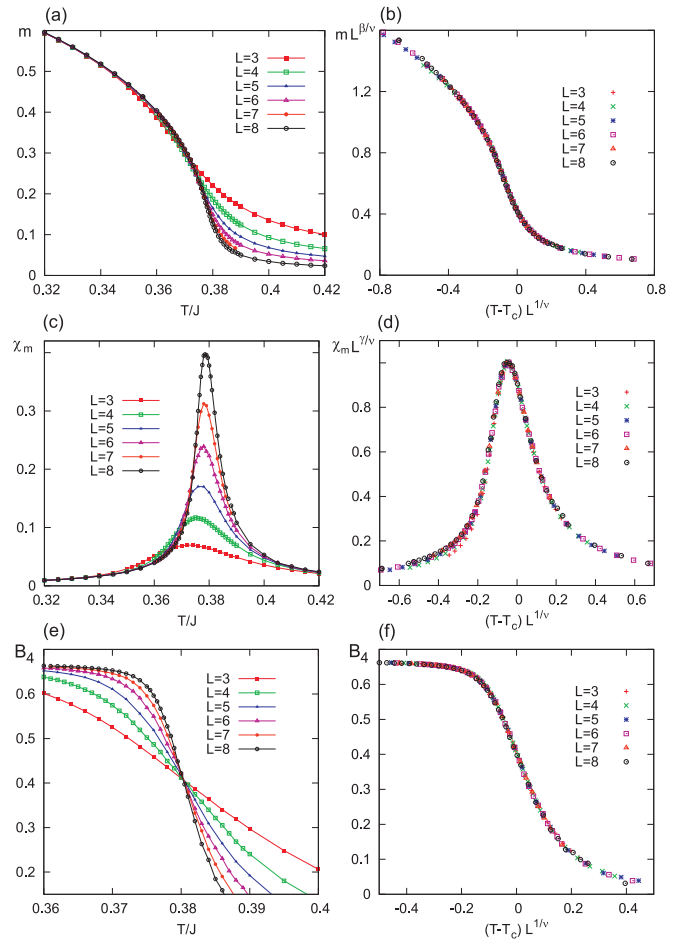


FIG. 4: The temperature dependence of (a) order parameter $|m|$, (c) susceptibility χ_m , and (e) Binder's cumulant B_{4m} obtained from Monte Carlo simulations for the specific case of $D = 0.14J$. The right panels (b), (d), and (f) show the corresponding finite-size scaling plots. The estimated critical exponents are $\beta = 0.38$, $\gamma = 1.121$ and $\nu = 0.63$.

The finite-size scaling plots shown in Figs. 4(b), (d), and (f) indicate that the data points indeed collapse on a universal curve. The critical exponents of the phase transition can be estimated from the corresponding scaling relations. For example, scaling of Binder's cumulant $B_{4m} = \mathcal{B}((T - T_c)L^{1/\nu})$ yields the critical exponent $\nu = 0.63$. Combined with the ratio α/ν obtained from the specific heat, we find $\alpha = 0.11$. Similarly, from the scaling of $|m|$ and χ_m , we obtain critical exponents $\beta = 0.38$ and $\gamma = 1.121$.

The discrete Z_2 symmetry of order parameter m implies a phase transition in the 3D Ising universality class. We found that the critical exponents α and ν indeed agree with the expected values for Ising transitions in three dimensions. The exponents β and γ , however, differ from the corresponding values of the 3D Ising class ($\beta = 0.32$ and $\gamma = 1.24$).²⁸ As discussed in Sec. I, this discrepancy could be caused by the dipolar-like effective interaction between spins in the Coulomb phase. Nonethe-

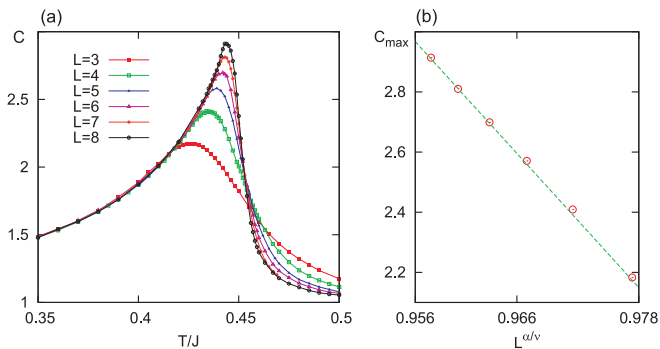


FIG. 5: Monte Carlo simulations for coupling constants $D = -0.7J$. (a) Specific heat $C = (\langle E^2 \rangle - \langle E \rangle^2) / NT^2$ as a function of temperature T . (b) The maximum of the specific heat C_{\max} as a function of $L^{\alpha/\nu}$, where $\alpha/\nu = -0.0217$.

less, the obtained exponents roughly satisfy the identity $\alpha + 2\beta + \gamma \approx 2$.

In Appendix B, we numerically study the magnetic ordering of Hamiltonian (1) assuming $J = 0$. As discussed in the previous section, the same all-in all-out magnetic order is selected as the ground state. Finite-size scaling analysis with the order parameter m shows that the magnetic phase transition indeed belongs to the 3D Ising universality class in the $J = 0$ limit. This contrasting result demonstrates that the discrepancy observed in exponents β and γ is attributed to the constraints imposed by a large J on the motion of spins in the Coulomb phase.

IV. XY-LIKE PHASE TRANSITION: INDIRECT DM INTERACTION

The indirect DM interaction only partially removes the magnetic frustration. At the single tetrahedron level, the degenerate ground-state manifold is parameterized by either ϕ or θ introduced in Eqs. (5) and (6), respectively. Nonetheless, the system undergoes a continuous phase transition at a temperature $T_c \sim \mathcal{O}(|D|)$. A clear peak can be seen in the temperature dependence of the specific heat as shown in Fig. 5(a). To characterize the phase transition, we need an order parameter which transforms as an irreducible representation of the symmetry group and properly describes the ground-state manifold.

To this end, we note that a general ground state of the indirect DM model can be constructed using the three orthogonal structures in which spins point along the $\langle 110 \rangle$ directions. We thus introduce unit vectors $\hat{\mathbf{m}}_{0,3}^c = (\mp 1, \pm 1, 0) / \sqrt{2}$ and $\hat{\mathbf{m}}_{1,2}^c = (\mp 1, \mp 1, 0) / \sqrt{2}$ for coplanar spins perpendicular to the c axis. Similar vectors $\hat{\mathbf{m}}_i^a$ and $\hat{\mathbf{m}}_i^b$ can be defined for the other two coplanar states. For a given spin configuration $\{\mathbf{S}_i\}$, the projection onto these orthogonal structures is given by

$$p_\mu = \frac{1}{NS} \sum_i \mathbf{S}_i \cdot \hat{\mathbf{m}}_i^\mu, \quad \mu = a, b, c. \quad (9)$$

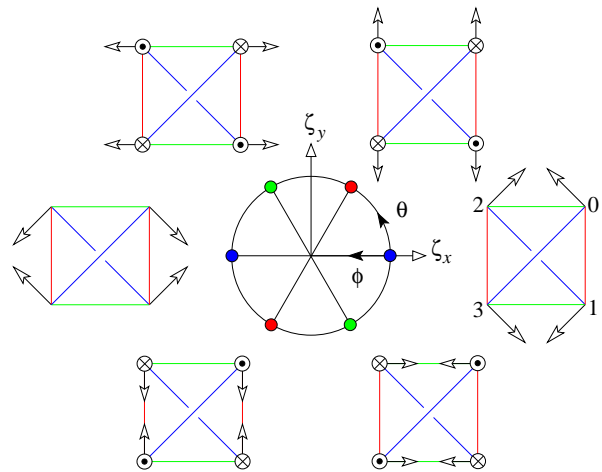


FIG. 6: The domain of the order parameter $\zeta = (\zeta_x, \zeta_y)$ is bounded by a circle whose circumference corresponds to non-coplanar ground states described by Eq. (6). The coplanar ground states given in Eq. (5) lies on the three straight lines $\zeta_y = \pm\sqrt{3}\zeta_x$ and $\zeta_y = 0$. Also shown are the six orthogonal magnetic structures where spins point along $\langle 110 \rangle$ directions; The \odot and \otimes symbols denote spin component coming out of and into the plane, respectively. They correspond to angles $\theta_\zeta = n\pi/3$ where $n = 0, \dots, 5$.

An order parameter $q = \max_\mu p_\mu^2$ was introduced in Ref. 26 to characterize the proximity of spin configurations to one of the six orthogonal structures shown in Fig. 6. Their Monte Carlo simulations demonstrated that q indeed approaches its maximum $q_{\max} = 1$ as $T \rightarrow 0$, indicating that the ground state consists of tetrahedra with orthogonal spins.

As already mentioned in Sec. I, the ordered phase has two distinct types of broken Z_6 symmetry. To characterize the different symmetry-breaking patterns, we introduce a two-component order parameter:

$$\zeta_x = (p_a + p_b - 2p_c) / \sqrt{6}, \quad \zeta_y = (p_a - p_b) / \sqrt{2}, \quad (10)$$

which transforms as the doublet representation of the group O_h . Note that the three projections are not independent as their symmetric sum $p_a + p_b + p_c$ vanishes identically. The domain of possible values of the vector $\zeta = (\zeta_x, \zeta_y)$ is bounded by a circle with radius $\sqrt{3}/2$ [Fig. 6]. Its circumference is made of noncoplanar ground states which are parameterized by θ [Eq. (6)]:

$$\zeta_x = \frac{\sqrt{3} \cos \theta}{\sqrt{2 + 4 \sin^2 \theta}}, \quad \zeta_y = \frac{3 \sin \theta}{\sqrt{2 + 4 \sin^2 \theta}}. \quad (11)$$

Noting that $\zeta_y/\zeta_x = \tan \theta_\zeta = \sqrt{3} \tan \theta$, the six orthogonal structures shown in Fig. 6 correspond to $\theta_\zeta = n\pi/3$ on the circumference, where $n = 0, \dots, 5$. These six states are the magnetic ground state at $T \rightarrow 0$.

Another set of degenerate ground states is given by the three straight lines $\zeta_y = \pm\sqrt{3}\zeta_x$ and $\zeta_y = 0$. They correspond to the coplanar spins described in Eq. (5); the

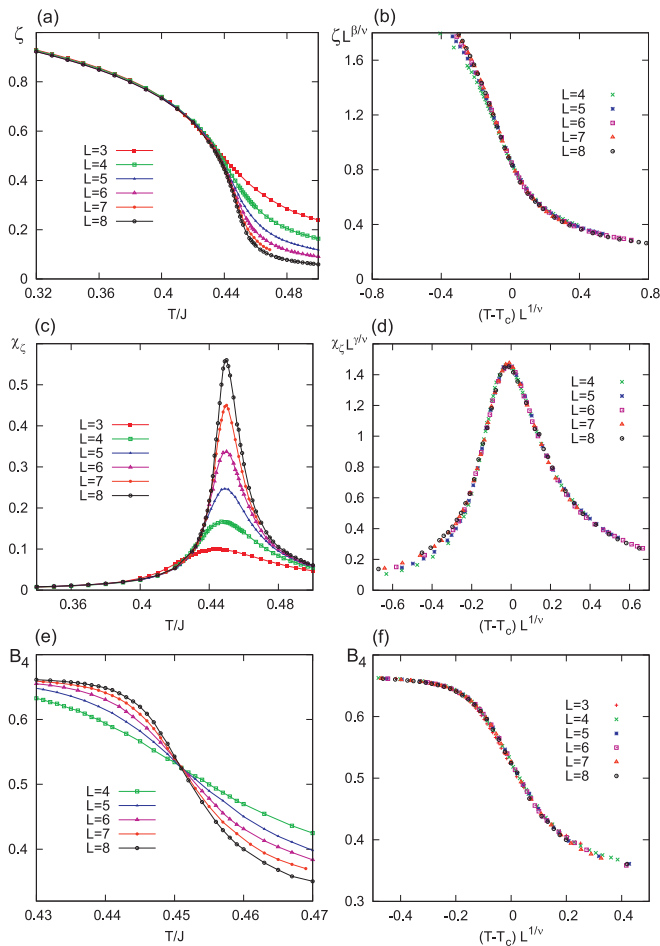


FIG. 7: The temperature dependence of (a) order parameter $\zeta = |\zeta|$, (c) susceptibility χ_ζ , and (e) Binder's cumulant $B_{4\zeta}$ obtained from Monte Carlo simulations for the specific case of $D = -0.7J$. The right panels (b), (d), and (f) show the corresponding finite-size scaling plots. The estimated critical exponents are $\beta = 0.42$, $\gamma = 1.181$, and $\nu = 0.672$.

order parameter of an orthogonal structure parameterized by ϕ is given by

$$\zeta_x = \sqrt{3/2} \cos \eta_\mu \cos \phi, \quad \zeta_y = \sqrt{3/2} \sin \eta_\mu \cos \phi, \quad (12)$$

where $\eta_{a/b} = \pm 2\pi/3$ and $\eta_c = 0$, and ϕ describes the global rotation of the coplanar spins about the corresponding cubic axes.

Fig. 7(a) shows the order parameter as a function of temperature obtained from Monte Carlo simulations. The amplitude $\langle |\zeta| \rangle$ of the order parameter increases markedly below a temperature $T_c \approx 0.45J$. In Figs. 7(c) and (e), we show the temperature dependence of the susceptibility and Binder's cumulant defined as

$$\chi_\zeta = \frac{N}{T} (\langle |\zeta|^2 \rangle - \langle |\zeta| \rangle^2), \quad B_{4\zeta} = 1 - \frac{\langle |\zeta|^4 \rangle}{3 \langle |\zeta|^2 \rangle^2}. \quad (13)$$

Again, a clear peak which diverges with the system size can be seen in the susceptibility curves. The crossing of

Binder's cumulants at a temperature $T_c \approx 0.452J$ indicates that the phase transition is second-order.

The order parameter ζ possesses a symmetry similar to that of XY model with a Z_6 anisotropy term. It is known that this anisotropy perturbation is dangerously irrelevant in 3D and the ordering transition is in the 3D XY universality class.²⁹⁻³² To investigate the nature of the observed phase transition, we performed finite-size scaling on the relevant quantities. The critical exponent ν which characterizes the scaling of correlation length can be estimated from the finite-size scaling plot of Binder's cumulant. As Fig. 7(f) shows, using $\nu = 0.672$ of the XY universality gives a rather good data collapsing. On the other hand, it is known that the XY model has a small negative exponent $\alpha = -0.0146$. The nonzero regular component of the specific heat makes its finite-size scaling a rather difficult task. Fig. 5(b) shows the maximum of the specific heat as a function of scaled system size: $C_{\max} = C_0 + \text{const} \times L^{\alpha/\nu}$. Using $\alpha/\nu = -0.0217$ from the XY universality class yields an agreeable result for large L .

The finite-size scaling plot of the order parameter [Fig. 7(b)] shows that the data points indeed fall on a universal curve $\zeta = L^{-\beta/\nu} \Phi((T - T_c)L^{1/\nu})$, from which we estimate the critical exponent $\beta = 0.42$. Similarly, scaling analysis of the susceptibility using relation $\chi_\zeta = L^{-\gamma/\nu} \Upsilon((T - T_c)L^{1/\nu})$ yields $\gamma = 1.181$. These two exponents differ from the expected values of 3D XY universality class ($\beta = 0.3485$ and $\gamma = 1.3177$).³³ As already discussed in the case of direct DM interaction, the discrepancy could be due to the constrained fluctuations of spins in the Coulomb phase. The long-range dipolar correlation of spins in this phase could modify the expected XY critical behavior. Nonetheless, the deviations in β and γ roughly compensate each other such that the critical exponents still satisfy the Rushbrooke equality $\alpha + 2\beta + \gamma \approx 2$.²⁸

V. ORDER-BY-DISORDER AND CROSSOVER PHENOMENON

A. Crossover between two types of Z_6 order

Although the order parameter ζ is indeed nonzero in the ordered phase, the pattern of the broken symmetry is unclear from the above Monte Carlo simulations. Expecting a state with broken Z_6 symmetry, we define another order parameter which is sensitive to the angular distribution of the vector ζ :^{34,35}

$$\zeta_6 = \langle |\zeta| \cos(6\theta_\zeta) \rangle, \quad (14)$$

where $\theta_\zeta = \arctan(\zeta_y/\zeta_x)$. The coplanar ground states with $\theta_\zeta = n\pi/3$ is characterized by a positive ζ_6 . In particular, a maximum $\zeta_{6,\max} = \sqrt{3/2}$ indicates that the system is in one of the six orthogonal structures shown in Fig. 6. We refer to this symmetry-breaking pattern

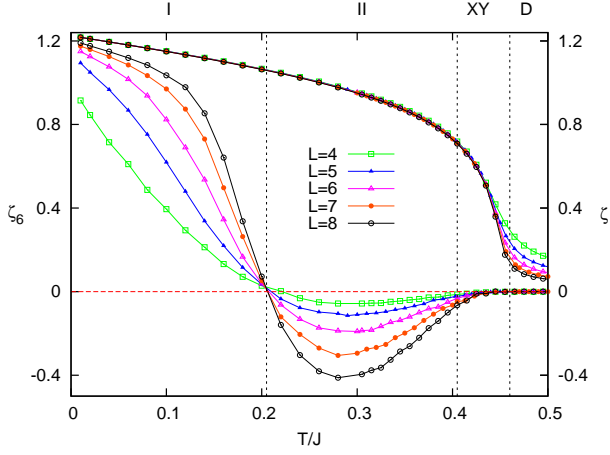


FIG. 8: Temperature dependence of the XY order parameter $\zeta = \langle |\zeta| \rangle$ and Z_6 order parameter ζ_6 for system size $L = 4, 5, 6, 7, 8$. The instantaneous distribution of the order parameter ζ in the four distinct regimes D, XY, I and II are shown in Fig. 9.

as the type-I order. Another type of broken Z_6 symmetry, referred to as the type-II order, corresponds to order parameter ζ clustered around the six angular positions $\theta_\zeta = (n + 1/2)\pi/3$. Tetrahedra in the type-II order consist of noncoplanar spins shown in Fig. 2(c). The Z_6 order parameter is negative $\zeta_6 < 0$ for the type-II order.

Fig. 8 shows the temperature dependence of the two order parameters ζ_6 and $\zeta = \langle |\zeta| \rangle$ obtained from Monte Carlo simulations. Depending on the angular distribution of the doublet vector ζ (shown in Fig. 9), we divide the ordered phase into three distinct regimes. In the XY regime just below T_c , the distribution of the order parameter exhibits an emergent rotational symmetry [Fig. 9(b)]. This result is consistent with numerical studies on the closely related 3D six-clock model which confirmed the irrelevance of the anisotropy at T_c .

Surprisingly, instead of directly settling in the type-I order which is shown to be the ground state as $T \rightarrow 0$ in Ref. 26, the system first enters a regime with type-II order as indicated by a negative ζ_6 . Upon further lowering the temperature, the system gradually switches to the type-I order. A crossover temperature can be estimated from the point where the order parameter ζ_6 changes sign. At $T \rightarrow 0$ the parameter ζ_6 approaches its maximum indicating a ground state with orthogonal spins.

As discussed in Sec. IV, the continuous degeneracy θ of the noncoplanar ground state corresponds to a rotational symmetry of the doublet vector ζ . As a result, the observed broken Z_6 symmetry, either the type-I or type-II order, must be of entropic origin. Naively, one would expect quantum or thermal fluctuations select the six orthogonal structures shown in Fig. 6 because they possess two zero modes corresponding to directions θ and ϕ in the ground-state manifold. By considering zero-point energy $\sum_m \varepsilon_m/2$ of magnons, Canals *et al.* showed that quantum fluctuations indeed favor the six orthogonal struc-

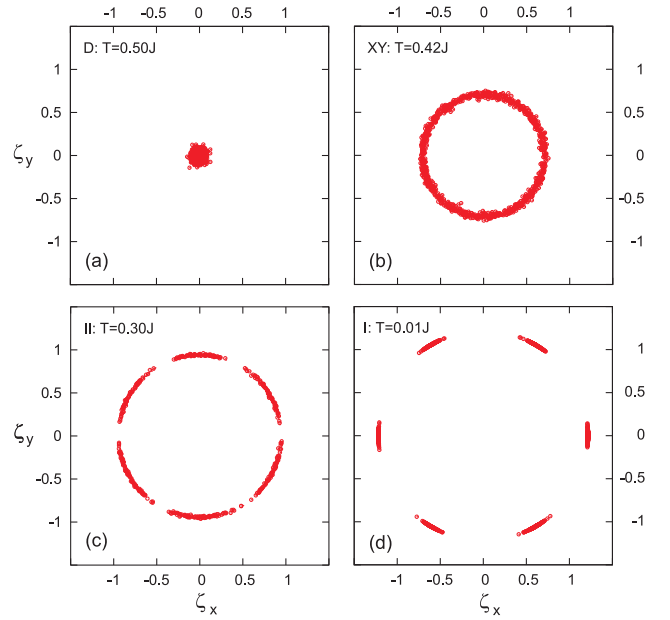


FIG. 9: Distribution of the instantaneous order parameter on the (ζ_x, ζ_y) plane for (a) disordered phase, (b) rotationally symmetric regime, (c) type-II and (d) type-I phases with broken Z_6 symmetry.

tures. However, at finite temperatures one must consider the magnon contribution to the system free energy. As we demonstrate below, the high-energy magnons actually play an important role in the high-temperature regime of the ordered phase.

B. Order from disorder: Holstein-Primakoff expansion

Here we compute the free energy due to the harmonic fluctuations around a given noncoplanar magnetic order. The free energy is a function of θ which parameterizes the $\mathbf{q} = 0$ noncoplanar spins given in Eq. (6). We first introduce a local reference frame defined by three orthonormal vectors: $\hat{\mathbf{e}}_i^x$, $\hat{\mathbf{e}}_i^y$, and $\hat{\mathbf{n}}_i$, which are functions of θ . A small deviation from the noncoplanar structure can be expressed using the Holstein-Primakoff expansion:

$$\mathbf{S}_i = S \left(1 - \frac{\sigma_i^2}{2S^2} \right) \hat{\mathbf{n}}_i + \sum_{a=x,y} \sigma_i^a \hat{\mathbf{e}}_i^a + \mathcal{O}(\sigma^3). \quad (15)$$

Here $\sigma_i = (\sigma_i^x, \sigma_i^y)$ whose components denote fluctuations along the two orthogonal local axes. Substituting the above expression into Eq. (1), we obtain a magnon Hamiltonian

$$\mathcal{H} = (J - \sqrt{2}D) \sum_i |\sigma_i|^2 + \sum_{i \neq j} \sum_{a,b=x,y} H_{ij}^{ab} \sigma_i^a \sigma_j^b, \quad (16)$$

where

$$H_{ij}^{ab} = \frac{1}{2} (J \hat{\mathbf{e}}_i^a \cdot \hat{\mathbf{e}}_j^b + \mathbf{D}_{ij} \cdot \hat{\mathbf{e}}_i^a \times \hat{\mathbf{e}}_j^b). \quad (17)$$

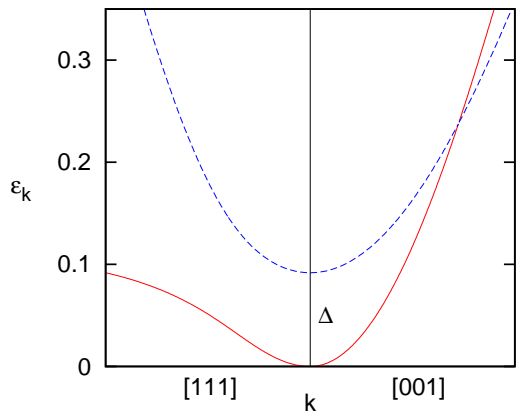


FIG. 10: Dispersion of the lowest two energy bands near the Γ point. The gapless band contains a zero mode at $\mathbf{k} = 0$ corresponding to the direction θ in the ground state manifold [c.f. Fig. 6]. The second band is gapped with $\Delta \sim D\theta^2$.

Since the noncoplanar structure is translationally invariant ($\mathbf{q} = 0$), the above Hamiltonian is diagonalized by Fourier transformation. In the vicinity of the coplanar state $\theta_\zeta = \theta = 0$, the lowest energy band has a gapless dispersion

$$\varepsilon_{1,\mathbf{k}} \approx \frac{1}{12}(2J + 5\sqrt{2}D)|\mathbf{k}_\perp|^2 + \frac{1}{6}(4J + \sqrt{2}D)k_z^2, \quad (18)$$

where $|\mathbf{k}_\perp|^2 = k_x^2 + k_y^2$. The zero mode at $\mathbf{k} = 0$ corresponds to the direction θ in the ground-state manifold [see Fig. 6]. The dispersion of the second lowest band is

$$\varepsilon_{2,\mathbf{k}} \approx \Delta + \frac{1}{4}(2J + \sqrt{2}D)|\mathbf{k}_\perp|^2 + \frac{D}{\sqrt{2}}k_z^2, \quad (19)$$

where the energy gap is due to a finite DM coefficient and is proportional to the deviation θ from the coplanar state:

$$\Delta \approx 4\sqrt{2}D\theta^2. \quad (20)$$

The vanishing of the gap at $\theta = 0$ corresponds to the zero mode described by the ϕ direction in Fig. 6, i.e. uniform rotation of spins about the cubic axes. At low temperatures, spin fluctuations are dominated by the low energy magnons. Due to the presence of two zero modes at $\theta = \phi = 0$, the six orthogonal structures shown in Fig. 6 are selected as the ground state as $T \rightarrow 0$, consistent with the Monte Carlo simulations.

At higher temperatures, one needs to take into account the contributions from the high energy bands. The magnon contribution to the free energy is given by

$$F_{\text{magnon}}(\theta_\zeta) = \sum_{n,\mathbf{k}} T \ln \sinh [\varepsilon_{n,\mathbf{k}}(\theta_\zeta)/T]. \quad (21)$$

The angle $\theta_\zeta = \arctan(\zeta_y/\zeta_x)$ is related to the parameter θ through $\tan \theta_\zeta = \sqrt{3} \tan \theta$. We numerically compute

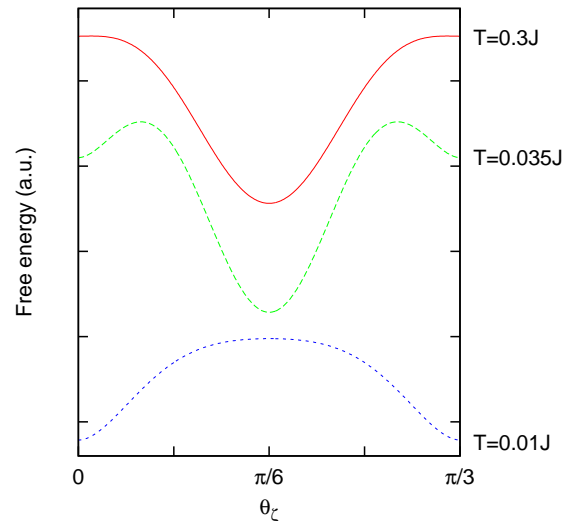


FIG. 11: Magnon free energy Eq. (21) as a function of angle $\theta_\zeta = \arctan(\zeta_y/\zeta_x)$. Note that this angle is related to the parameter θ characterizing a general noncoplanar structure [Eq. (6)] through $\tan \theta_\zeta = \sqrt{3} \tan \theta$. The coupling constant used in the calculation is $D = -0.2J$. Note that $\theta_\zeta = \pi/6$ corresponds to noncoplanar structure shown in Fig. 2(c), whereas $\theta_\zeta = 0$ and $\pi/3$ correspond to orthogonal spins shown in Figs. 6 and 2(b).

the free energy by summing over states within the Brillouin zone. Fig. 11 shows the free energy as a function of θ_ζ . At higher temperatures, e.g. $T = 0.3J$, the minimum of F_{magnon} occurs at $\theta_\zeta = (n + 1/2)\pi/3$ corresponding to noncoplanar spins shown in Fig. 2(c). As the temperature decreases, local minimum starts to develop at angles $\theta_\zeta = n\pi/3$ which correspond to the six orthogonal structures shown in Fig. 6 or Fig. 2(b). As temperature is further lowered, the orthogonal magnetic order takes over and becomes the absolute minimum of the free energy. This calculation clearly shows that thermal fluctuations favor two distinct spin structures at different temperatures of the ordered phase, as indeed observed in Monte Carlo simulations.

VI. CONCLUSION

To summarize, we have studied the critical behavior of a classical pyrochlore antiferromagnet with Dzyaloshinskii-Moriya interactions. Symmetry considerations allow for two distinct forms of antisymmetric coupling on the pyrochlore lattice which are termed direct and indirect DM interactions.^{25,26} The macroscopic degeneracy of the nearest-neighbor Heisenberg spins is lifted for both types of DM interaction. Through extensive Monte Carlo simulations, we have demonstrated the continuous nature of magnetic ordering in both cases. The critical exponents of the phase transitions were obtained from finite-size scaling analysis. Finally, we have

shown that the ordered phase in the indirect DM model exhibits two distinct types of broken Z_6 symmetry.

The direct DM interaction completely relieves the geometrical frustration and selects a doubly degenerate all-in all-out magnetic order. We have observed an Ising-like phase transition with critical exponents $\alpha = 0.11$, $\beta = 0.38$, $\gamma = 1.121$, and $\nu = 0.63$. The deviation from the expected 3D Ising universality is attributed to the correlated spin fluctuations in the Coulomb phase. This is because minimization of the nearest-neighbor exchange requires the total spin on every tetrahedra be zero, which in turn results in a dipolar-like spin correlation at large distances. As is well known, the long-range dipolar spin interaction could modify the nature of the magnetic phase transition.

We have also simulated a pyrochlore magnet where the only coupling between spins is the nearest-neighbor DM interaction. Noting that this model selects exactly the same all-in all-out ground state, we have shown that the corresponding magnetic transition indeed belongs to the 3D Ising universality class when spin fluctuations are not subject to local constraints imposed by the nearest-neighbor exchange.

To characterize the symmetry-breaking phase of the indirect DM model, we have introduced a doublet order parameter ζ . The domain of this doublet vector is bounded by a circle whose circumference is composed of degenerate noncoplanar ground states. On the other hand, coplanar ground states with spins perpendicular to one of the cubic axes lie on the lines $\zeta_y = \pm\sqrt{3}\zeta_x$ and $\zeta_y = 0$. Finite-size scaling analysis using the doublet order parameter yields a set of critical exponents: $\alpha = -0.0146$, $\beta = 0.42$, $\gamma = 1.181$, and $\nu = 0.672$. Similar to the case of direct DM interaction, we have observed noticeable deviations in β and γ from the expected 3D XY universality class. Again, the dipolar spin correlation in the Coulomb phase can cause the observed discrepancy.

Our simulations have also uncovered an unusual order from disorder phenomenon in the case of indirect DM interaction. Thermal fluctuations below the transition temperature lift the continuous degeneracy and select a $\mathbf{q} = 0$ magnetic order with six-fold degeneracy. Interestingly, the magnet first develops a noncoplanar magnetic order before settling in the coplanar ground state. The crossover between these two types of Z_6 order corresponds to a rotation of the doublet vector ζ from $\theta_\zeta = (n + 1/2)\pi/3$ to $\theta_\zeta = n\pi/3$, where n is an integer. By computing the magnon contribution to the free energy, we have explicitly demonstrated that the observed crossover indeed originates from the entropic selection.

Acknowledgments

I thank E. Choi, N. Perkins, C. Fennie, and O. Tchernyshyov for collaboration on related works.

Appendix A: Continuum approximation

Here we outline a continuum description of the pyrochlore antiferromagnet with DM interaction. Following Refs. 4 and 5, we define a magnetic or polarization field at the center of a tetrahedron as

$$\mathbf{B}^a = \sum_{i \in \mathbb{T}} S_i^a \hat{\mathbf{e}}_i, \quad (\text{A1})$$

where $\hat{\mathbf{e}}_i$ denotes the local $\langle 111 \rangle$ direction at site i . Comparing with the definition of the three staggered magnetizations, we observe

$$\mathbf{B}^a = 4S(L_1^a, L_2^a, L_3^a). \quad (\text{A2})$$

This relation was first noted in Ref. 27. In the coarse-grained approximation, the constraint $\mathbf{M} = 0$ translates to $\nabla \cdot \mathbf{B}^a(\mathbf{r}) = 0$ for each component a . Expressed in terms of the staggered fields, we have

$$\partial_x L_1^a + \partial_y L_2^a + \partial_z L_3^a = 0. \quad (\text{A3})$$

Noting that the states with small values of \mathbf{B}^a are entropically favored, the probability distribution of the flux field has a Gaussian distribution, i.e. $\rho \propto e^{-\mathcal{H}_{2a}}$ with

$$\mathcal{H}_{2a} = \frac{\kappa}{2} \int d^3\mathbf{r} \sum_i |\mathbf{L}_i(\mathbf{r})|^2. \quad (\text{A4})$$

The stiffness κ is the single parameter of the theory which controls the amplitude of the correlations. The correlators of the staggered magnetizations at large distances are

$$\langle L_i^a(\mathbf{r}) L_j^b(0) \rangle \propto \frac{\delta_{ab}}{\kappa} \frac{r^2 \delta_{ij} - 3r_i r_j}{r^5}. \quad (\text{A5})$$

While \mathcal{H}_{2a} is entirely of entropic origin, an additional energy term comes from the DM interaction

$$\begin{aligned} \mathcal{H}_{2b} = & -\mathcal{D} \int d^3\mathbf{r} \left[\hat{\mathbf{a}} \cdot \mathbf{L}_2(\mathbf{r}) \times \mathbf{L}_3(\mathbf{r}) \right. \\ & \left. + \hat{\mathbf{b}} \cdot \mathbf{L}_3(\mathbf{r}) \times \mathbf{L}_1(\mathbf{r}) + \hat{\mathbf{c}} \cdot \mathbf{L}_1(\mathbf{r}) \times \mathbf{L}_2(\mathbf{r}) \right], \end{aligned} \quad (\text{A6})$$

where the coupling constant $\mathcal{D} \propto DS^2$. The competition between the two terms leads to a phase transition into an ordered phase with nonzero $\langle \mathbf{L}_i(\mathbf{r}) \rangle$. Details of the staggered fields are discussed in Sec. II for the two different forms of DM interaction.

To ensure stability of the ordered phase and give penalties to short-wavelength fluctuations, we add gradient and quartic terms

$$\mathcal{H}_{2c} = \int d^3\mathbf{r} \sum_i \left[A_1 |\nabla \cdot \mathbf{L}_i(\mathbf{r})|^2 + A_2 |\nabla \times \mathbf{L}_i(\mathbf{r})|^2 \right], \quad (\text{A7})$$

$$\mathcal{H}_4 = \int d^3\mathbf{r} \left[u \sum_i |\mathbf{L}_i(\mathbf{r})|^4 + v \sum_{i \neq j} |\mathbf{L}_i(\mathbf{r})|^2 |\mathbf{L}_j(\mathbf{r})|^2 \right]. \quad (\text{A8})$$

The sum $\mathcal{H}_2 + \mathcal{H}_4$ thus constitute a continuum framework for describing the phase transition induced by DM interactions. Although the resultant expression resembles a conventional Landau-Ginzburg-Wilson functional expressed in terms of the antiferromagnetic order parameters, it is important to note that these order parameter fields are not independent. Instead, they are subject to the constraint (A3). This condition can be satisfied by introducing a vector field $\mathbf{A}^a = (A_1^a, A_2^a, A_3^a)$ for each spin component a such that $\mathbf{B}^a = \nabla \times \mathbf{A}^a$. Regrouping the vector potentials $\tilde{\mathbf{A}}_i = (A_i^x, A_i^y, A_i^z)$, the coarse-grained staggered fields is given by

$$\mathbf{L}_i(\mathbf{r}) = \epsilon_{ijk} \partial_j \tilde{\mathbf{A}}_k(\mathbf{r}) \quad (\text{A9})$$

A detailed analysis of the resulting energy functional in terms of $\tilde{\mathbf{A}}_k(\mathbf{r})$ will be presented in future publications.

Appendix B: Ising transition in direct DM model with $J = 0$

In this appendix, we examine the critical behavior of classical Heisenberg spins with direct DM interaction alone on the pyrochlore lattice:

$$\mathcal{H} = \sum_{\langle ij \rangle} \mathbf{D}_{ij} \cdot (\mathbf{S}_i \times \mathbf{S}_j) \quad (\text{B1})$$

This model corresponds to the special case $J = 0$ of the Hamiltonian (1) studied in the main text. Remarkably, the anisotropic direct DM interaction alone selects the same all-in all-out magnetic ground state [Fig. 2(a)] as in the $J \rightarrow \infty$ limit. However, since spin fluctuations are not subject to constraints $\sum_{i \in \boxtimes} \delta \mathbf{S}_i = 0$ imposed by a large J , this model provides us an opportunity to examine how the universality class of the magnetic transition is modified by the long-range dipolar correlation of spins in the Coulomb phase.

Fig. 12(a) shows the specific heat as a function of temperature. A clear peak which diverges with increasing

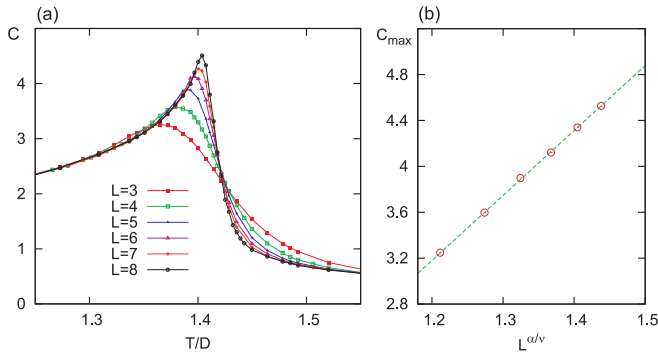


FIG. 12: (a) Specific heat C as a function of temperature T for various system sizes. (b) The maximum of the specific heat C_{\max} as a function of $L^{\alpha/\nu}$, where $\alpha/\nu = 0.175$. The number of spins $N = 16L^3$ for a system with linear size L .

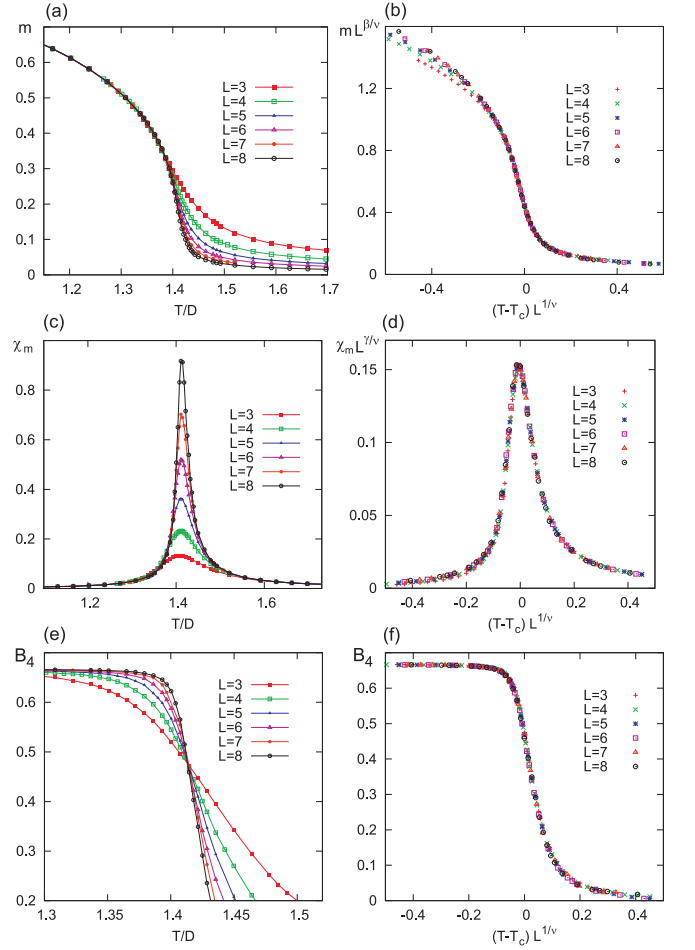


FIG. 13: The temperature dependence of (a) order parameter $|m|$, (c) susceptibility χ_m , and (e) Binder's cumulant B_{4m} obtained from Monte Carlo simulations. The right panels (b), (d), and (f) show the corresponding finite-size scaling plots with 3D Ising critical exponents: $\beta = 0.32$, $\gamma = 1.24$ and $\nu = 0.63$.

system sizes indicates a continuous phase transition at $T_c \sim \mathcal{O}(D)$. Due to the existence of nonzero regular component in the specific heat, finite-size scaling of C is rather difficult. Fig. 12(b) shows the maximum of specific-heat as a function of $L^{\alpha/\nu}$, where we have used the ratio $\alpha/\nu = 0.175$ from 3D Ising universality class. The data collapsing on a straight line indicates a scaling relation $C_{\max} = C_0 + \text{const} \times L^{\alpha/\nu}$. We use the same order parameter m defined in Eq. (7) to characterize the doubly degenerate all-in all-out magnetic order. The temperature dependence of m and the corresponding susceptibility and Binder's cumulant are shown in Fig. 13. Using critical exponents of 3D Ising universality: $\beta = 0.32$, $\gamma = 1.24$, and $\nu = 0.63$, we obtained excellent data collapsing as shown in the corresponding finite-size scaling plots [Fig. 13]. The analysis shows that without the constraints imposed by nearest-neighbor exchange J , the phase transition into the doubly degenerate all-in all-out state indeed belongs to 3D Ising class.

-
- ¹ R. Moessner and A. P. Ramirez, *Physics Today* **59** (2), 24 (2006).
- ² R. Moessner and J. T. Chalker, *Phys. Rev. Lett.* **80**, 2929 (1998); *Phys. Rev. B* **58**, 12049 (1998).
- ³ M. Hermele, M. P. A. Fisher, and L. Balents, *Phys. Rev. B* **69**, 064404 (2004).
- ⁴ S. V. Isakov, K. Gregor, R. Moessner, and S. L. Sondhi, *Phys. Rev. Lett.* **93**, 167204 (2004).
- ⁵ C. L. Henley, *Phys. Rev. B* **71**, 014424 (2005).
- ⁶ S.-H. Lee, C. Broholm, T. H. Kim, W. Ratcliff II, and S.-W. Cheong, *Phys. Rev. Lett.* **84**, 3718 (2000).
- ⁷ J.-H. Chung, M. Matsuda, S.-H. Lee, K. Kakurai, H. Ueda, T. J. Sato, H. Takagi, K.-P. Hong, and S. Park, *Phys. Rev. Lett.* **95**, 247204 (2005).
- ⁸ R. G. Melko, B. C. den Hertog, M. J. P. Gingras, *Phys. Rev. Lett.* **87**, 067203 (2001).
- ⁹ O. Cepas, A. P. Young, B. S. Shastry, *Phys. Rev. B* **72**, 184408 (2005).
- ¹⁰ T. S. Pickles, T. E. Saunders, J. T. Chalker, *Europhys. Lett.* **84** 36002 (2008).
- ¹¹ T. E. Saunders, J. T. Chalker, *Physical Review B* **77**, 214438 (2008).
- ¹² D. Tsuneishi, M. Ioki, and H. Kawamura, *J. Phys. Condens. Matter*, **19**, 145273 (2007).
- ¹³ G.-W. Chern, R. Moessner, and O. Tchernyshyov, *Phys. Rev. B* **78**, 144418 (2008).
- ¹⁴ E. Brézin, J. C. Le Guillou, and J. Zinn-Justin, *Phys. Rev. B* **10**, 892 (1974).
- ¹⁵ P. Bak, S. Krinsky, and D. Mukamel, *Phys. Rev. Lett.* **36**, 52 (1976).
- ¹⁶ A. I. Larkin and D. E. Khmel'nitskii, *Sov. Phys. JETP* **29**, 1123 (1969).
- ¹⁷ A. Aharony, *Phys. Rev. B* **8**, 3363 (1973).
- ¹⁸ J. N. Reimers, A. J. Berlinsky, and A.-C. Shi, *Phys. Rev. B* **43**, 865 (1991).
- ¹⁹ J. N. Reimers, J. E. Greedan, and M. Bjorgvinsson, *Phys. Rev. B* **45**, 7295 (1992).
- ²⁰ I. E. Dzyaloshinskii, *Sov. Phys. JETP* **19**, 960 (1964).
- ²¹ T. Moriya, *Phys. Rev.* **120**, 91 (1960).
- ²² G.-W. Chern, C. Fennie, and O. Tchernyshyov, *Phys. Rev. B* **74**, 060405(R) (2006).
- ²³ O. Tchernyshyov and G.-W. Chern, in *Highly Frustrated Magnetism*, edited by C. Lacroix, P. Mendels, and F. Mila (Springer, 2010).
- ²⁴ Y. Onose, T. Ideue, H. Katsura, Y. Shiomi, N. Nagaosa, Y. Tokura, *Science* **329**, 297 (2010).
- ²⁵ M. Elhajal, B. Canals, R. Sunyer, and C. Lacroix, *Phys. Rev. B* **71**, 094420 (2005).
- ²⁶ B. Canals, M. Elhajal, and C. Lacroix, *Phys. Rev. B* **78**, 214431 (2008).
- ²⁷ P. H. Conlon, J. T. Chalker, *Phys. Rev. B* **81**, 224413 (2010).
- ²⁸ P. M. Chaikin and T. C. Lubensky, *Principles of Condensed Matter Physics* (Cambridge University Press, Cambridge, 2000).
- ²⁹ J. V. Jose, L. P. Kadanoff, S. Kirkpatrick, and D. R. Nelson, *Phys. Rev. B* **16**, 1217 (1977).
- ³⁰ M. Oshikawa, *Phys. Rev. B* **61**, 3430 (2000).
- ³¹ P. D. Scholten and L. J. Irakliotis, *Phys. Rev. B* **48**, 1291 (1993).
- ³² J. Hove and A. Sudbo, *Phys. Rev. E* **68**, 046107 (2003).
- ³³ M. Campostrini, M. Hasenbusch, A. Pelissetto, P. Rossi, and E. Vicari, *Phys. Rev. B* **63**, 214503 (2001).
- ³⁴ R. K. Heilmann, J.-S. Wang, R. H. Swendsen, *Phys. Rev. B* **53**, 2210 (1996).
- ³⁵ J. Lou, A. W. Sandvik, L. Balents, *Phys. Rev. Lett.* **99**, 207203 (2007).